Journal of Energy Storage 54 (2022) 105315

Contents lists available at ScienceDirect

Journal of Energy Storage

journal homepage: www.elsevier.com/locate/est

Research papers

Heat transfer performance of a device integrating thermosyphon with form-stable phase change materials

Wei Zhong [a], Wandong Min [a], Xiaoling Cao [a], Nan Zhang [a], Ziyu Leng [a], Yanping Yuan [a,*], Shady Attia [b]

[a] School of Mechanical Engineering, Southwest Jiaotong University, Chengdu, China
[b] Sustainable Building Design Lab, Department UEE, Faculty of Applied Sciences, Université de Liège, Belgium

ARTICLE INFO

Keywords:
Heat transfer
Thermal storage
PCM
Phase transition
Passive thermal transport
Energy storage

ABSTRACT

Phase change materials (PCM) are applied worldwide as a thermal energy storage technology to reduce energy demands in buildings and solve environmental contamination issues. Form-stable phase change materials (FSPCM), as one branch of PCMs, can be improved by embedding them with thermosyphon, resulting in a better thermal performance. In this paper, a novel thermoplastic elastomer-based FSPCM was developed and tested. A device integrating FSPCM with thermosyphon was created, and the heat transfer mechanism of the unit was studied. The numerical model was established, and experiments were conducted accordingly. The average relative error between the experimental data and the model predictions was <3 %. Furthermore, a parameter study was conducted to investigate the effects of several essential factors. As a result, the evaporator length and PCM thermal conductivity were found to significantly influence the unit's heat transfer rate and overall thermal performance. However, the impact of the latent heat of the FSPCM on the heat transfer rate was negligible, for which it takes 1170 s, 1230 s, and 1394 s to finish changing phase with 136 kJ/kg, 160 kJ/kg, and 200 kJ/kg, respectively. This paper provides insights on the performance of thermosyphon integrated form-stable phase change materials and discusses its relevance for thermal energy storage applications.

1. Introduction

Energy demand and environmental contaminants represent significant challenges in daily life, particularly in the building and manufacturing fields, accompanied by economic enhancement and social development [1]. A wide range of techniques and high-efficiency energy systems have been explored and implemented, reducing pollution and saving energy [2]. Among these innovative technologies, thermal energy storage is recognized as one of the most efficient approaches for sustainable control and energy utilization. Meanwhile, as a dominant carrier of thermal energy, phase change materials (PCMs) are applied worldwide because of their high energy storage density, chemical, and thermal stability, nearly absent supercooling properties, and capacity of passive heat storage at a near-constant phase change temperature [3].

Form-stable phase change materials (FSPCMs), as one branch of PCMs, can effectively prevent irreversible damage caused by liquid leakages and are currently attracting widespread attention from researchers [4,5]. They have the following virtues: (1) low requirements or no need for sealing techniques with extra containers compared to regular liquid-solid PCM, resulting in low costs and easy manufacturing; (2) the volume alteration of the material is minor, and the expansion coefficient is generally low; (3) they have stable thermal and physical performance with outstanding reliability; (4) the material can be implemented and recycled in the industry straightforwardly and conveniently [6]. Relevant work has been conducted in different application fields (e.g., solar energy systems [7], energy storage systems for buildings [8], passive thermal management of batteries [9], photovoltaic electricity generation [10], cold storage [11], etc.). However, the low thermal conductivity of FSPCM during the phase change process hinders its practical application [12]. Once the heat transfer performance inside the materials can be improved, FSPCM can be adopted as an economical, efficient, and simple material for commercialization.

To improve the thermal conductivity and performance of the latent heat thermal energy storage materials, various advanced techniques, such as adding fins [13], embedding heat pipes [14], filling metal foams

* Corresponding author.
E-mail address: ypyuan@home.swjtu.edu.cn (Y. Yuan).

https://doi.org/10.1016/j.est.2022.105315
Received 9 March 2022; Received in revised form 29 June 2022; Accepted 12 July 2022
Available online 18 July 2022

[15], or nanoparticles [16], have been explored and analyzed. Among these approaches, heat pipes (HPs) incorporated with PCMs are usually effectively applied in diverse applications as thermal saving units to improve the overall thermal performance of systems [17]. Thus far, Naghavi et al. [18], Rashidi et al. [2]., and Etheridge et al. [19] have reviewed and summarized the traditional heat pipe associated with PCMs. The relevant research indicated that heat pipes possess excellent heat transfer ability and high efficiency in improving heat transfer within PCMs. Moreover, they can diminish the total thermal resistance if incorporated into a neat PCM system, resulting in an integrated system maintaining sizeable thermal conductivity and latent heat capacity. A thermosyphon (TS), i.e., a specific heat pipe without a wick attached to the inner wall, is also adopted to improve the PCM heat transfer performance. It is promoted in many applications, including HVAC systems [20], solar energy systems [21], battery cooling [22], and so on. Zhong and Ji [23] reviewed and summarized relevant works, and they pointed out that TS/PCM systems have similar advantages to the HP/PCM system. However, the mechanism of heat transfer and interaction between PCM and TS lacks sufficient study, and the numerical and economic analysis of the system is inadequate as well.

To the best of the 'authors' knowledge, thermosyphon's transient heat transfer process is rarely investigated when attaching FSPCM to the condenser side as an unsteady temperature boundary condition. Moreover, the overall thermal performance of this novel integrated unit needs to be evaluated and optimized. This hybrid heat storage device can be used for heat recovery in the industry field as the waste flue gas/water is relatively high as 60–70 °C. Besides, 'it's also appropriate for solar photovoltaic/thermal (PV/T) technology to improve its efficiency. In this paper, a thermoplastic elastomer-based FSPCM consisting of paraffin wax (PW), an olefin block copolymer (OBC), expanded graphite (EG), and Styrene-b-(ethylene-co-butylene)-b-styrene (SEBS) was prepared and studied due to its good thermal conductivity and reasonable latent heat capacity. The theory and concept of the TS/FSPCM unit were introduced, and then the numerical model of the TS/PCM unit was built and demonstrated. Moreover, experiments were conducted to observe the TS/FSPCM unit's heat transfer performance and verify the simulation's accuracy. Furthermore, the effects of several essential parameters (i.e., the evaporator length, the thermal conductivity, and latent heat of FSPCM) were investigated by the numerical approach to better understand the heat transfer phenomenon of the TS/FSPCM unit. These results are expected to provide a new basis for the heat transfer analysis of the TS/FSPCM unit and encourage the development of relevant thermal energy storage applications.

2. Theory and numerical model of thermosyphons and PCMs

To comprehensively simulate the heat transfer performance of the TS/FSPCM unit shown in Fig. 1, the heat transfer processes in TS and PCM are first separately presented in this section. Then, the integrated model is demonstrated and explained based on energy conservation. The model can predict the heat transfer process through the thermosyphon to the PCM section, including sensible and latent heat transfer.

2.1. Numerical model of the heat transfer process of TS

A traditional closed two-phase thermosyphon is usually placed vertically, consisting of an evacuated bare tube with the working fluid inside [24]. In the thermosyphon, no capillary structure exists compared to the traditional wick heat pipe. Heat is absorbed in the bottom of the tube, known as the evaporator section, where the liquid will be vaporized and then flow to the top of the device. The heat can be released in the condenser section so that the vapor will condense. During the condensation procedure, the liquid returns by gravity and accumulates into a thin film attached to the inner wall of the tube. Thus, thermosyphons are recognized as good low-resistance heat transfer devices because of the high efficiency of the latent heat transfer of the liquid-vapor phase change.

For decades, the mechanism of thermosyphons has been extensively

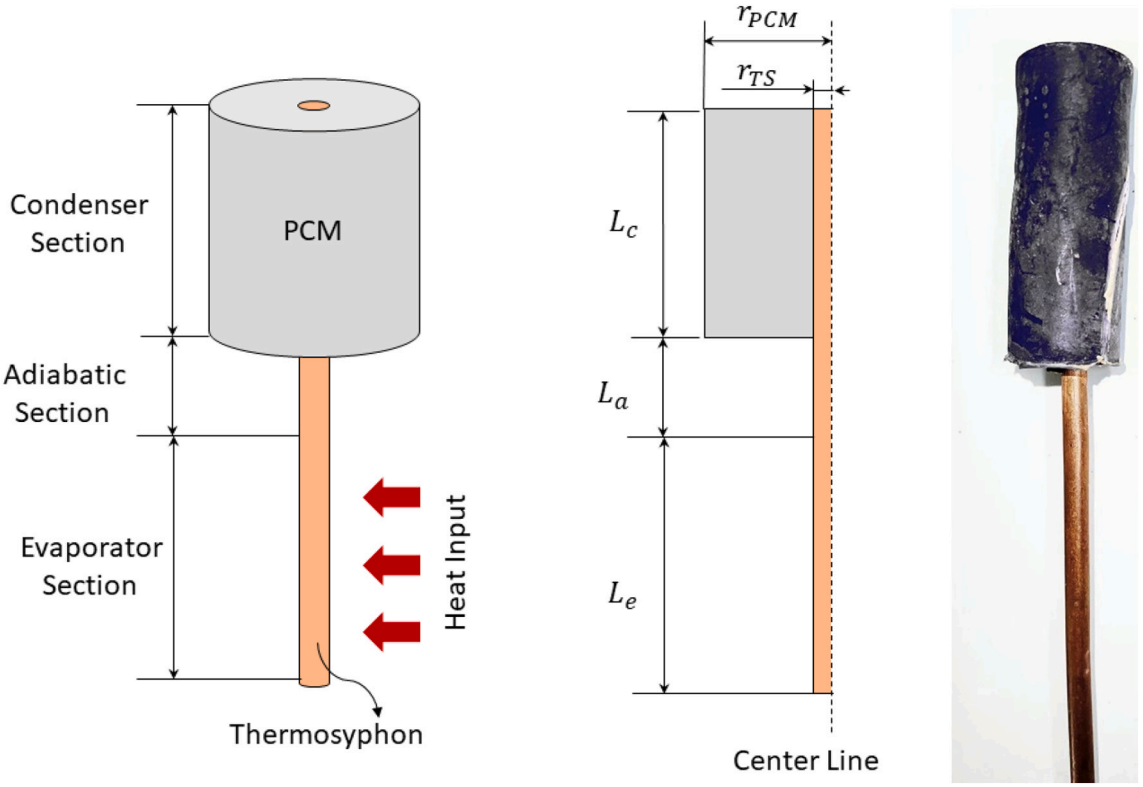

Fig. 1. Diagram of the TS with FSPCM unit.

investigated. Typical limits of traditional thermosyphons are listed as follows when the heat input is high enough: counter-current flooding (or entrainment) limit [25,26], dry-out limit [27,28], pool boiling limit [29], viscous limit [30], burn-out or film-boiling limit [31], and sonic limit [32]. The heat transfer performance of each section of TS has been well studied for various applications and situations. In this paper, the simulation of the thermosyphon section is built based on Zhong et al.'s's [33] model, which considers the heat transfer in the condenser and evaporator individually.

To predict the condensation resistance inside the TS when the film thickness is unknown, the heat transfer coefficient of the condenser section can be expressed according to [34]. The average Nusselt number ($\overline{Nu_c}$) is provided by

$$Re_\delta = 4P\frac{\overline{h_c}\left(\frac{v_l^2}{g}\right)^{1/3}}{k_l} = 4P\overline{Nu_c} \tag{1}$$

where $\overline{h_c}$ is the average heat transfer coefficient of the condensation process in TS, g is the gravity constant, and Re_δ is the Reynolds number of the film. k_l and v_l are the thermal conductivity and kinematic viscosity of the working fluid inside the TS, respectively. The dimensionless parameter P is

$$P = \frac{k_l L_c (T_v - T_c)}{\mu_l h_{fg}\left(\frac{v_l^2}{g}\right)^{1/3}} \tag{2}$$

where L_c is the length of the condenser section; μ_l and h_{fg} are the dynamic viscosity and the latent heat of the working fluid, correspondingly. T_v is the saturated vapor temperature, and T_c is the condenser inner wall temperature. The average Nusselt numbers in terms of P are yielded as follows:

$$\begin{aligned} \overline{Nu_c} &= 0.943\ P^{-1/4}\ P \le 15.8 \\ \overline{Nu_c} &= \frac{1}{P}(0.68P + 0.89)^{0.82}\ 15.8 < P \le 2530 \\ \overline{Nu_c} &= \frac{1}{P}\left[(0.024P - 53)Pr_l^{1/2} + 89\right]^{4/3}\ P > 2530, Pr_l \ge 1 \end{aligned} \tag{3}$$

where Pr_l is the Prandtl number of the working fluid at the liquid phase.

The equation given by Imura [35] is implemented to calculate the average heat transfer coefficient of the evaporator($\overline{h_e}$), which takes the effects of pressure inside TS into consideration.

$$\overline{h_e} = 0.32\left(\frac{\rho_l^{0.65} k_l^{0.3} Cp_l^{0.7} g^{0.2} q_e^{0.4}}{\rho_v^{0.25} h_{fg}^{0.4} \mu_l^{0.1}}\right)\left(\frac{P_v}{P_a}\right)^{0.3} \tag{4}$$

where Cp_l and μ_l are the specific heat and dynamic viscosity of the working fluid at the liquid phase, correspondingly. q_e is the heat flux in the evaporator section. P_v and ρ_v are the saturated pressure and the density of the working fluid at the vapor phase, respectively. P_a is the ambient pressure.

In this paper, the heat transfer limits are considered as well according to eq. 17 to 19 from reference [33].

2.2. Numerical model of melting process of PCM

A phase change material can release and absorb energy to heat and cool at the phase transition. Many works have studied the numerical simulation of PCM's transient phase change process. In this paper, due to the geometry of PCM and TS, a one-dimensional thermal resistance and capacity model is selected to predict the heat transfer performance of the melting process of form-stable PCM, and several assumptions are made as follows:

1) The thermal conductivity of form-stable PCM remains consistent as the temperature varies;
2) Natural convection in composite PCM is neglected because there is no liquid phase during the phase change process;
3) The density of composite PCM is considered to be constant;
4) The heat only transfers along the radius direction, which reduces the model to a 1D simulation.

The basic governing equation of heat transfer is presented below:

$$Cp \bullet m\frac{\partial T}{\partial t} = k\frac{\partial^2 T}{\partial x^2} \tag{5}$$

Assume that the radius of the PCM is divided into n discrete sections, as shown in Fig. 2, and the thickness of each discrete section is set as $\delta(=(r_{PCM} - r_{TS})/n)$. Based on the energy balance equation and Fourier law, discrete expressions are given by

$$\begin{aligned} &Cp_{PCM,i} \bullet m_{PCM,i}\frac{T_{PCM,i} - T^0_{PCM,i}}{dt} = \frac{T_{cond} - T_{PCM,i}}{R_{i,a}} - \frac{T_{PCM,i} - T_{PCM,i,i+1}}{R_{i,b}}, i = 1 \\ &Cp_{PCM,i} \bullet m_{PCM,i}\frac{T_{PCM,i} - T^0_{PCM,i}}{dt} = \frac{T_{PCM,i-1,i} - T_{PCM,i}}{R_{i,a}} - \frac{T_{PCM,i} - T_{PCM,i,i+1}}{R_{i,b}}, \\ &i = 2,3,4.....n-1 \\ &Cp_{PCM,i} \bullet m_{PCM,i}\frac{T_{PCM,i} - T^0_{PCM,i}}{dt} = \frac{T_{PCM,i,i-1} - \mathrm{T}_{PCM,i}}{R_{i,a}}, i = n \end{aligned} \tag{6}$$

where $m_{PCM,\ i}$ and $T_{PCM,\ i}$ represent the mass and temperature of each element of the PCM, respectively. T_{cond} is the outer wall temperature of the condenser. $T_{PCM,\ i,\ i+1}$ is the interface temperature between element i and i+1, which can be calculated by

$$T_{PCM,i,i+1} = \frac{R_{i,b}}{R_{i+1,a} + R_{i,b}}T_{PCM,i+1} + \frac{R_{i+1,a}}{R_{i+1,a} + R_{i,b}}T_{PCM,i}, i = 1,2,3....n-1 \tag{7}$$

$R_{i,\ a}$ and $R_{i,\ b}$ stand for the thermal resistance of the discrete PCM due to the conduction, which can be rewritten as

$$\begin{aligned} R_{i,a} &= \frac{ln\dfrac{r_{TS} + \dfrac{2i-1}{2}\delta}{r_{TS} + (i-1)\delta}}{2\pi k_{pcm}} \\ R_{i,b} &= \frac{ln\dfrac{r_{TS} + i\delta}{r_{TS} + \dfrac{2i-1}{2}\delta}}{2\pi k_{pcm}} \end{aligned} \tag{8}$$

Considering the phase transition process, the effective specific heat capacity ($Cp_{PCM,\ i}$) is defined as

$$Cp_{PCM,i} = \begin{cases} Cp_{PCM}, T_{PCM,i} \le T_m - \sigma \\ Cp_{PCM} + \dfrac{H_{fg}}{2\sigma}, T_m - \sigma < T_{PCM,i} < T_m + \sigma \\ Cp_{PCM}, T_{PCM,i} \ge T_m + \sigma \end{cases} \tag{9}$$

where T_m and σ are the phase change temperature and temperature interval of the PCM, correspondingly. H_{fg} is the latent heat of the PCM.

2.3. Integrated numerical model of thermosyphons with PCMs

In Fig. 2, a basic working schematic of the TS/FSPCM unit is presented. The working fluid absorbs heat from the heat input and evaporates to vapor. The vapor flows along the tube and condenses in the condenser section, in which heat can be released to the PCM by thermal conduction. After heat dissipation, the working fluid is cooled and returns to the bottom of the TS. The condenser heats the PCM, and the

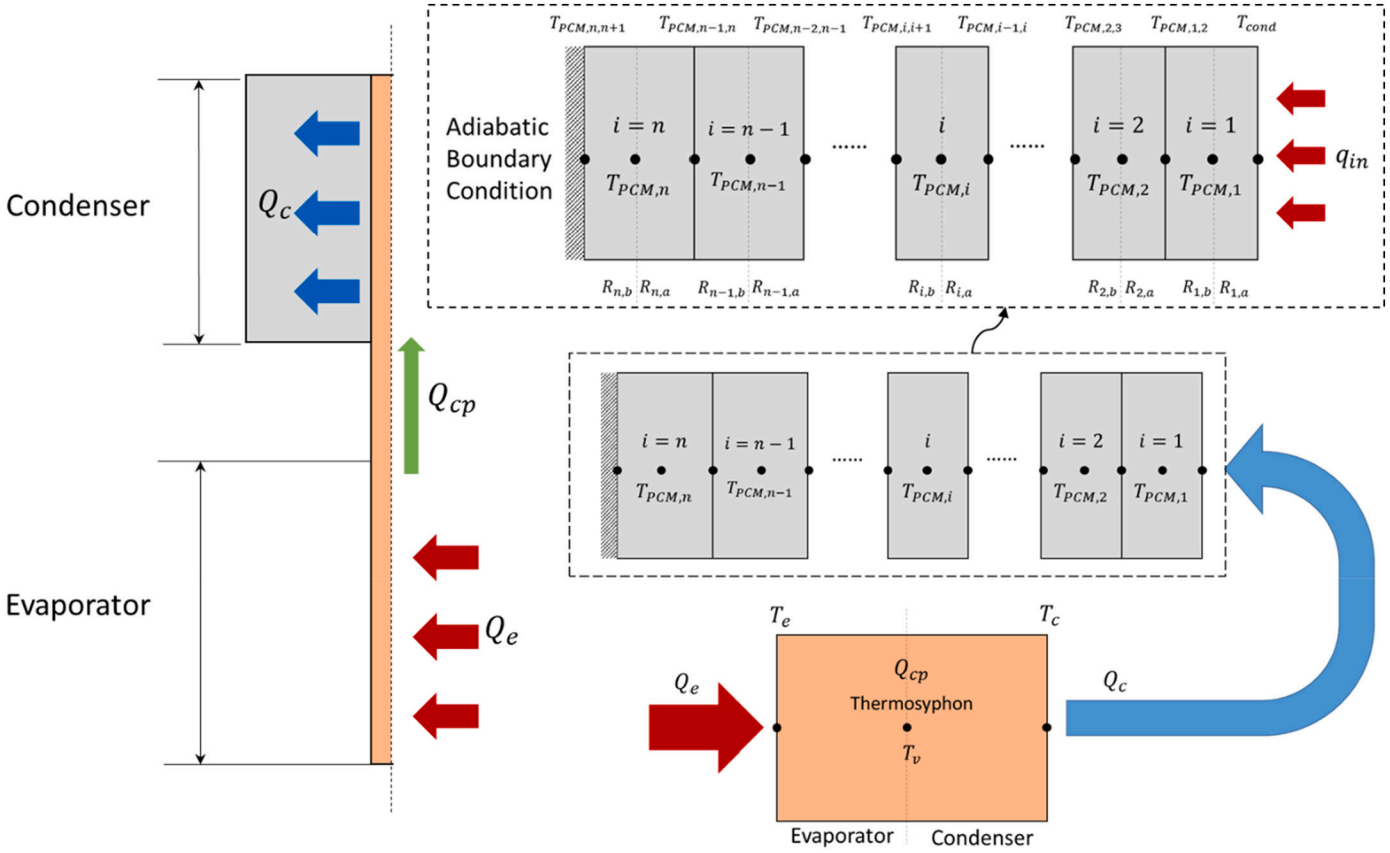

Fig. 2. Schematic of 1D-RC model.

heat is transferred and stored. Regarding the heat transfer process via TS and PCM demonstrated above, some assumptions are made as follows:

1) The thermal resistance of the thermosyphon wall is neglected due to the high thermal conductivity of the metal material;
2) The thermophysical properties of the wall of the thermosyphon remain constant;
3) There is no heat loss during the heat transfer process via TS to PCM.

Thus, in order to investigate the thermal distribution of the TS/FSPCM unit, the integrated numerical model can be built based on the energy conservation equation as illuminated in Fig. 2,

$$\begin{aligned} Q_e &= A_e(T_e - T_v)\overline{h_e} = Q_c + Q_{cp} \\ &= A_c(T_c - T_v)\overline{h_c} + \left(Cp_{wf}m_{wf} + Cp_{wall}m_{wall}\right)\left(T_v - T_v^0\right) \end{aligned} \tag{10}$$

where Q_e, Q_c, and Q_{cp} represent the heat absorbed by the evaporator, which is equal to the total heat input, the heat released by the condenser—which then transfers to the PCM section—and the sensible heat due to the temperature variation of thermosyphon, correspondingly. A_e and A_c are the total surface areas of the evaporator and condenser sections, respectively.

As the PCM absorbs heat from the condenser section of TS, the boundary temperature of the PCM equals the condenser wall temperature ($T_c = T_{cond}$), and the heat flux at the interface between PCM and TS should be the same ($q_{in} = q_c$), which also can be expressed as

$$q_{in} = \frac{T_{cond} - T_{PCM,i}}{R_{1,a}} = \frac{Q_c}{L_c 2\pi \bullet r_{TS}} \tag{11}$$

Organizing the discrete equation creates a tridiagonal matrix for the PCM section. Then, the Thomas algorithm is applied to the Matlab code to complete the calculation. The flow chart of the numerical solution for PCM integrated with TS is shown in Fig. 3.

3. Experimental analysis

3.1. Experiment set-up

The TS/FSPCM unit consists of a thermosyphon and PCM sections. As shown in Fig. 4, a customized container made of aluminum alloy was used to locate the temperature sensors and hold the form-stable PCM. The thermosyphon was embedded in the center of the PCM, which was made of copper and charged with water. Moreover, the evaporator section was vertically placed in a water heating bath (HH-2, LICHEN, Shanghai, China), providing the heating boundary condition as a constant temperature condition. The adiabatic section of TS and the outer wall of the container were covered by insulation to eliminate heat loss.

After setting the evaporator section into the water bath, the heat is absorbed from the water by the phase change of the working fluid inside TS due to the temperature difference between the evaporator and the condenser section. Annd then the heat is transferred to the PCM section by conduction. As the PCM stores the heat, the temperature of the PCM varies from the initial state (i.e., atmosphere temperature). By recording the temperature data, the heat transfer performance of the TS/FSPCM system could be analyzed. The geometry and conditions of the system are demonstrated in Table 1.

3.2. Data acquisition

The TS/FSPCM system was verified experimentally by observing the temperature distribution in the PCM section, measured by a temperature sensor (K-WRNK-191, Chenyi, Hanzhou, China) with ±0.1 °C accuracy. As shown in Fig. 5, the four sensors were evenly attached to the 'evaporator's outer surface from top to bottom, and two were placed in the

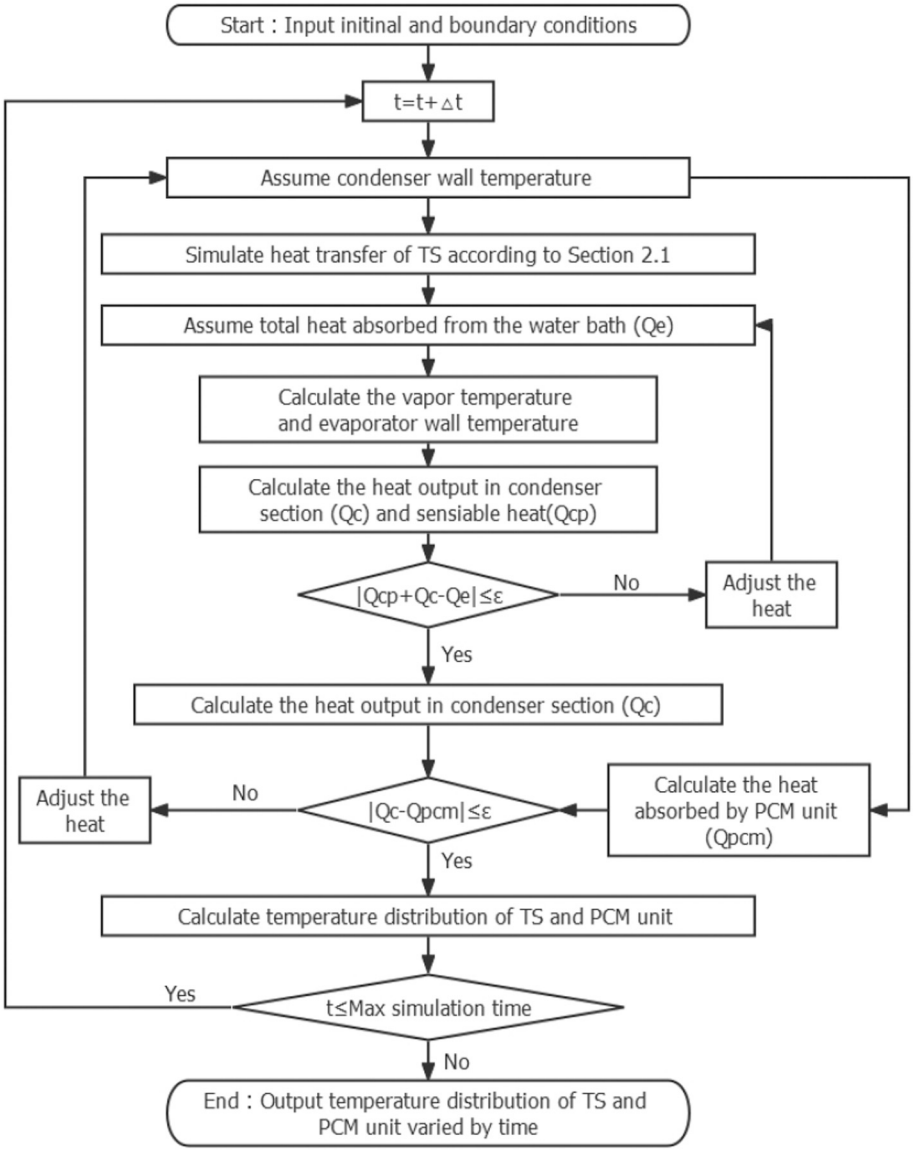

Fig. 3. Flowchart of the numerical solution.

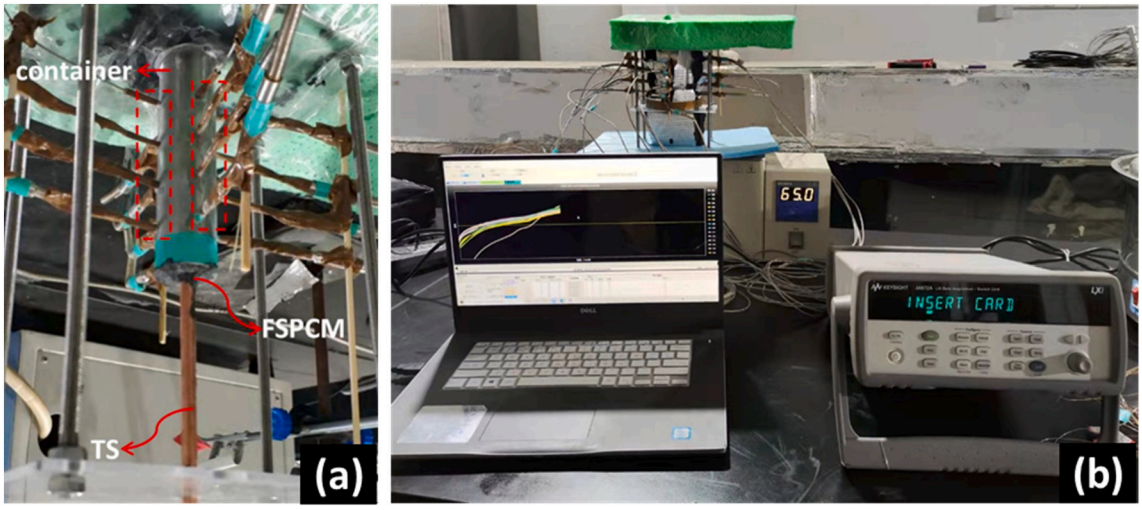

Fig. 4. Experimental set-up of TS/FSPCM. (a) TS/FSPCM unit; the temperature sensors are located in the red dashed box. (b) Overview of the whole system. (For interpretation of the references to colour in this figure legend, the reader is referred to the web version of this article.)

Table 1
The geometry of the TS/FSPCM unit.

Description	Value
Length of 'thermosyphon's condenser section	100 mm
Length of 'thermosyphon's evaporator section	100 mm
Length of 'thermosyphon's adiabatic section	100 mm
Diameter of thermosyphon	6 mm
Diameter of the container	20 mm
Filling ratio of thermosyphon	6 %
Water bath temperature	65 °C
Ambient air temperature	12.5 °C

adiabatic section. Four sections were divided in the PCM container, which is illuminated in Fig. 5 (b). Moreover, in each section, by controlling the distance between the probe of the temperature sensor and the outer surface of the condenser, there were four temperature measurement points. In other words, the temperature at the location a (1A, 2B, 3C, and 4D), which was 4.4 mm away from the thermosyphon outer wall, should be consistent according to the assumption made in Section 2, for which the heat only transfers along the radius direction; the same applies to location b (1B, 2C, 3D, 4A), location c (1C, 2D, 3A, 4B), and location d (1D, 2A, 3B, 4C), respectively (Fig. 6). The data were collected using a data acquisition instrument (KEYSIGHT-34972A, Keysight Technologies, CA, USA). During the overall test process, all temperatures were recorded at an interval of 1 s.

3.3. Preparation and properties of FSPCM

The FSPCM was improved according to the material introduced in reference [36] with a phase change temperature of 36–40 °C. It was made of paraffin wax (PW) (melting temperature: 41–44 °C), an olefin block copolymer (OBC) (INFUSETM 9530, company of DOW, USA), expanded graphite (EG), and Styrene-b-(ethylene-co-butylene)-b-styrene (SEBS) (FG1901, 30/70, company of Kraton, USA), and the composition of the FSPCM is indicated in Table 2.

To produce the FSPCM, PW and SEBS were first melt-blended under 100 °C and stirred for twenty minutes at 50–80 rpm. When the solution became homogeneous and transparent, OBC was added to the composition, and the temperature was increased to 180 °C with stirring at 120 rpm for 30 min. When the solution became homogeneous and transparent again, EG was implemented in the solution to increase the thermal conductivity of the PCM, also at 180 °C and stirred at 120 rpm. When the composition reaches a uniform state, pouring it into the container to cool (Fig. 7). The specific thermophysical properties of the FSPCM were measured and are given in Table 3.

4. Results and discussion

4.1. Grid and time-step independence of the model

Regarding the grid size and time-step strongly influencing the accuracy and efficiency of the numerical simulation, various calculations with different grid sizes and time steps are compared in this paper to optimize the prediction process. As a result, the temperature profile of PCM at $r = 100$ mm under different grid sizes and time steps is indicated in Fig. 8. Considering the need for acceptable accuracy and reasonable efficiency, $\delta = 0.2$ mm and $dt = 1$ s are selected for further study.

4.2. Validation of the numerical model

The validation of the simulation model for the TS/FSPCM unit is illuminated in Fig. 9, in which the red lines represent the simulation results and black lines stand for experimental data. The measured temperature of location a is the average temperature at locations 1A, 2B, 3C, and 4D, given as an example. The experiments were conducted under the same conditions several times, and the results showed good consistency. Quantitative error analysis was implemented for the temperatures of the FSPCM at different locations between simulation and experiment in Eq. (12)–(14), consisting of the normalized mean bias error (NMBE), root means square error (RMSE), and average relative error (ARE) [37]. The results are listed in Table 4, and they were generally <3 %.

$$NMBE = \sum_{k=1}^{m} |T_{sim}(k) - T_{exp}(k)| \Big/ \left(\overline{T_{exp}(k)} \bullet m\right) \times 100\% \quad (12)$$

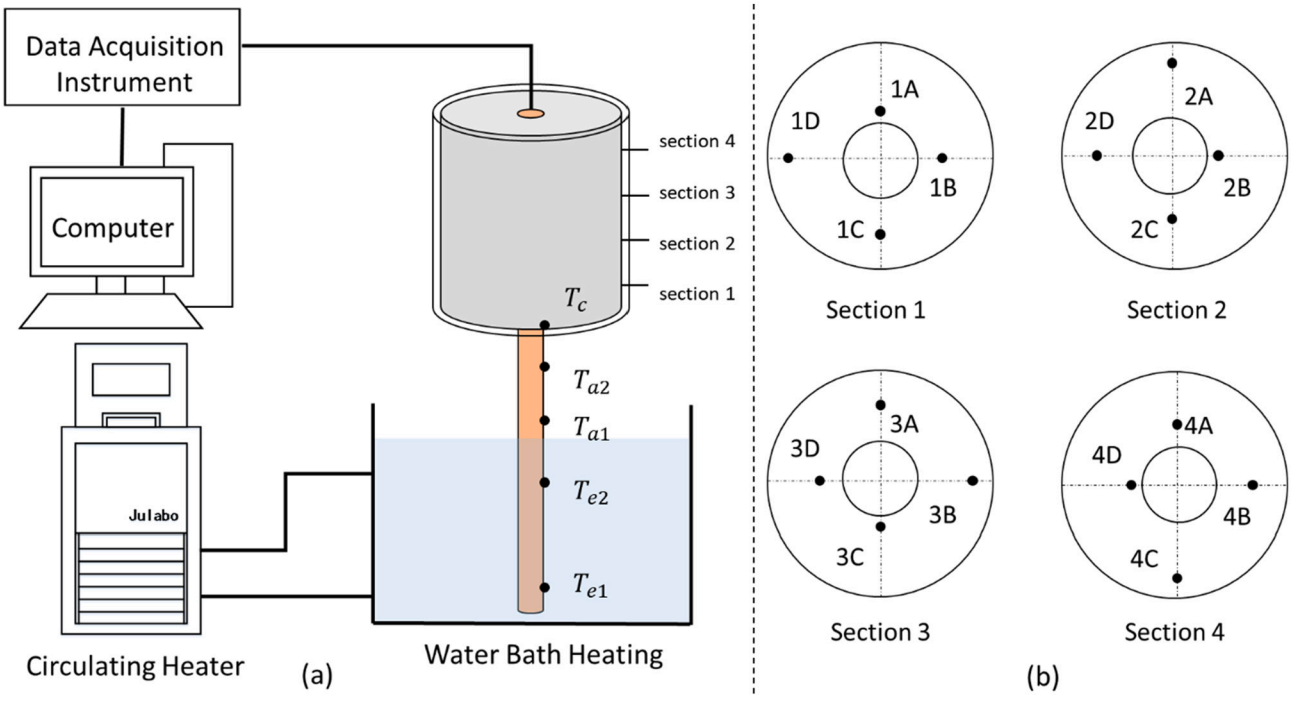

Fig. 5. Schematic of the thermosyphon test set-up. (a) Schematic of key components. (b) Details of the temperature measurement point.

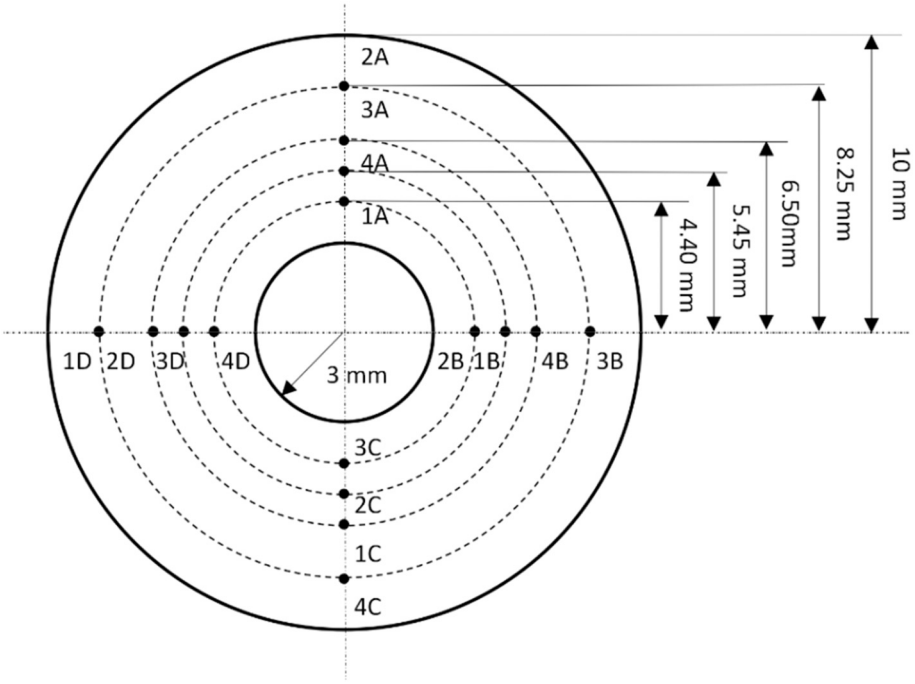

Fig. 6. The temperature sensor locations in the vertical view.

Table 2
The composition of the FSPCM.

Composite	PW	SEBS	OBC	EG
Mass ratio	80.7 %	5.6 %	11.4 %	2.3 %

$$RMSE = \sqrt{\frac{\sum_{k=1}^{m}\left(T_{sim}(k) - T_{exp}(k)\right)^2}{m}} \Big/ \overline{T_{exp}(k)} \times 100\% \tag{13}$$

$$ARE = \frac{\sum_{k=1}^{m}\left|\left(T_{sim}(k) - T_{exp}(k)\right) \Big/ T_{exp}(k)\right|}{m} \tag{14}$$

As shown in Fig. 9, the trend of the temperature distribution of the FSPCM varied with time, which was correctly captured with an acceptable deviation. The results indicate that the temperature rises at first due to sensible heat transfer, and then remains at a constant level for a period due to the latent heat of the phase change, and increases again to reach the condenser wall temperature finally. The major distinction between the simulation and experimental data is located from 1300 s to 2000 s, which represents the completion of the phase change, and the temperature rises due to sensible heat transfer. The temperature differences among locations a, b, c, and d in the experiment are larger than those in the simulation, and this is because heat loss during the transfer process is ignored in the simulation. The temperature is higher for the experiment compared with the simulation at location a at $t = 2000$s. This is mainly due to the thermal conductivity of the FSPCM decreasing with increasing temperature for the real case; thus, the higher thermal resistance of the PCM is established. Meanwhile, the constant thermal conductivity is implemented during the simulation, taking the value at 45 °C of the FSPCM according to Table 3. More experiments with varying evaporator lengths were conducted compared with the simulation in the following sections. Thus, it could be concluded that the simulation model has reasonable accuracy and could

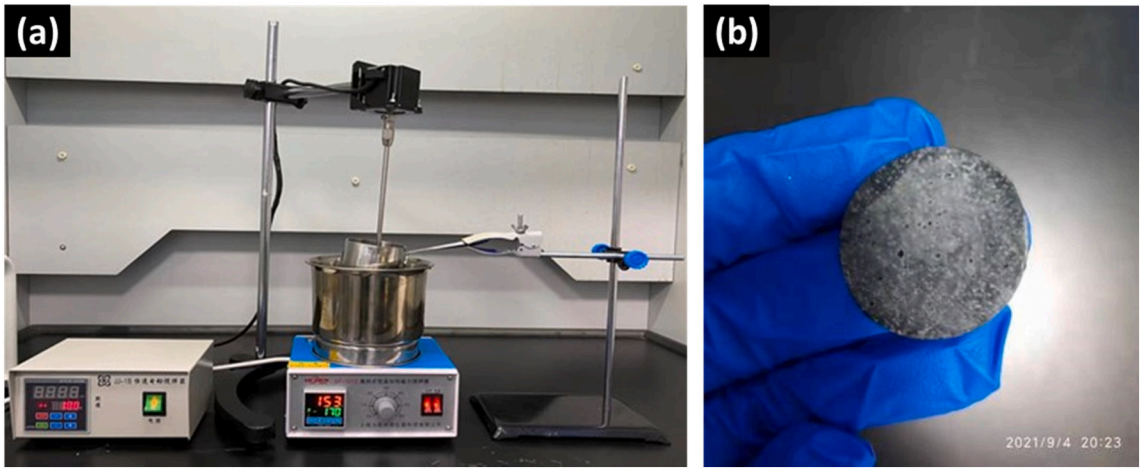

Fig. 7. (a) Apparatus to generate the form-stable PCM. (b) The form-stable PCM sample was implemented for this paper.

Table 3
Thermo-physical properties of FSPCM.

Property	Value
Phase-change-onset temperature	36 °C
Phase-change-end temperature	40 °C
Latent heat of fusion	136 kJ/kg
Specific heat capacity (at 30 °C)	2389 J/(kg•K)
Specific heat capacity (at 45 °C)	1896 J/(kg•K)
Thermal conductivity (at 30 °C)	0.747 W/(m•K)
Thermal conductivity (at 45 °C)	0.368 W/(m•K)
Leaking rate (at 60 °C)	0.83 %
Density at 20 °C (solid)	689 kg/m^3

be used to predict the heat transfer performance of the TS/FSPCM unit.

4.3. Results analysis

According to the experimental data and simulation results in Fig. 9, three stages can be distinguished based on the state of the FSPCM to describe the heat transfer process of the TS/FSPCM unit when it starts to store heat.

- Stage 1: The phase change fraction of the FSPCM remains 0, which means that only sensible heat transfer occurred in this period. As placing the TS into the water bath, the FSPCM started to absorb heat through the TS, and the temperature of the FSPCM increased rapidly at first due to the material's high thermal conductivity, as shown in Table 3.
- Stage 2: The phase change fraction increased from 0 to 1. This means that the phase change covers the whole process, and the latent heat is dominant for heat storage. When the material began to change phase, there was a stage with a near-constant temperature for each location.
- Stage 3: The phase change fraction reached one and remained consistent. This indicates that the phase change process had been completed and sensible heat dominated again. After completing the phase change process, the temperature started to rise again slowly and tended to reach a value equal to the temperature of the thermospyhon's condenser wall.

In summary, in the macroscopic view, only thermal conductance took place in the FSPCM when the heat was transferred via TS to PCM. Due to the heat capacity, there is a temperature lag for transient heat transfer along the radius direction of PCM. At the same time, the closer the location to the TS condenser wall, the higher the temperature of the material. As the boundary condition of heat input can be regarded as a constant temperature condition, the heat storage flux in the FSPCM at each moment is mainly reliant on the temperature difference (ΔT_{TS}) between the condenser and evaporator. When the heat accumulates near the condenser side of the FSPCM, the temperature at r = 30 mm increases, which restricts the heat transfer capacity of the device. As a result, the heat flux decreases with time due to the decline in ΔT_{TS}.

To better understand the process of phase change in the TS/PCM unit, the simulation results of the temperature distribution and phase change fraction varying with time are demonstrated in Fig. 10 and Fig. 11. In stage 1, from 0 to around 150 s, the major heat absorbed in the PCM was sensible heat, which was related to the material's heat capacity. The heat was driven to transfer to the PCM via TS when placing TS in the water bath. This is because of the temperature difference between the initial temperature of the PCM (12.5 °C) and the water bath

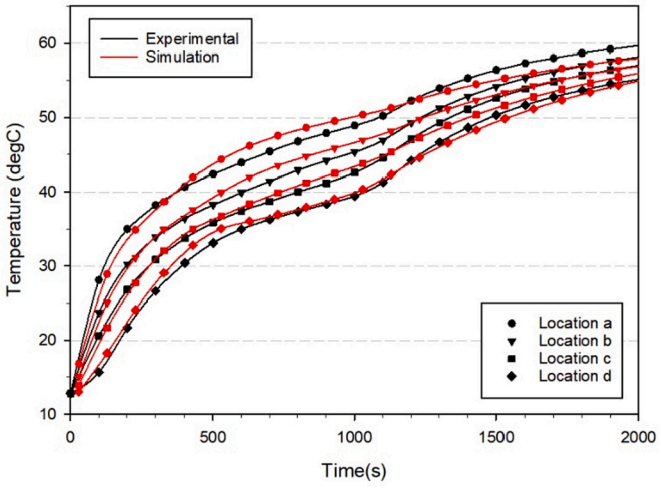

Fig. 9. Validation of experimental data and simulation of TS/FSPCM unit.

Table 4
NMBE, RMSE, and ARE values for model validation.

	Location a	Location b	Location c	Location d
Normalized mean bias error (NMBE)	2.62 %	2.81 %	2.95 %	3.16 %
Root mean square error (RMSE)	2.84 %	2.46 %	2.14 %	1.94 %
Average relative error (ARE)	2.87 %	2.38 %	1.99 %	2.02 %

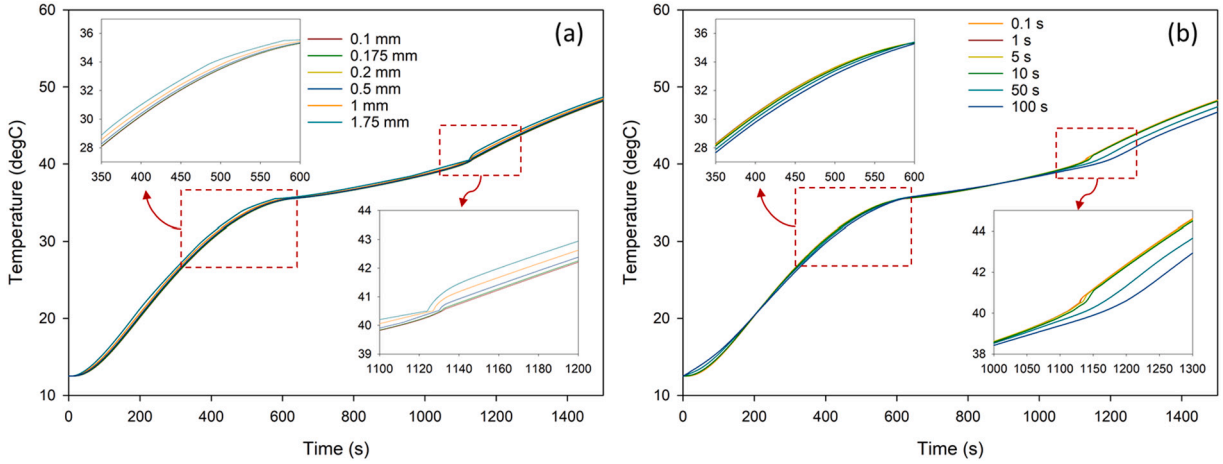

Fig. 8. (a) Temperature profile of PCM at r = 100 mm under different grid numbers. (b) Temperature profile of PCM at r = 100 mm under different time steps.

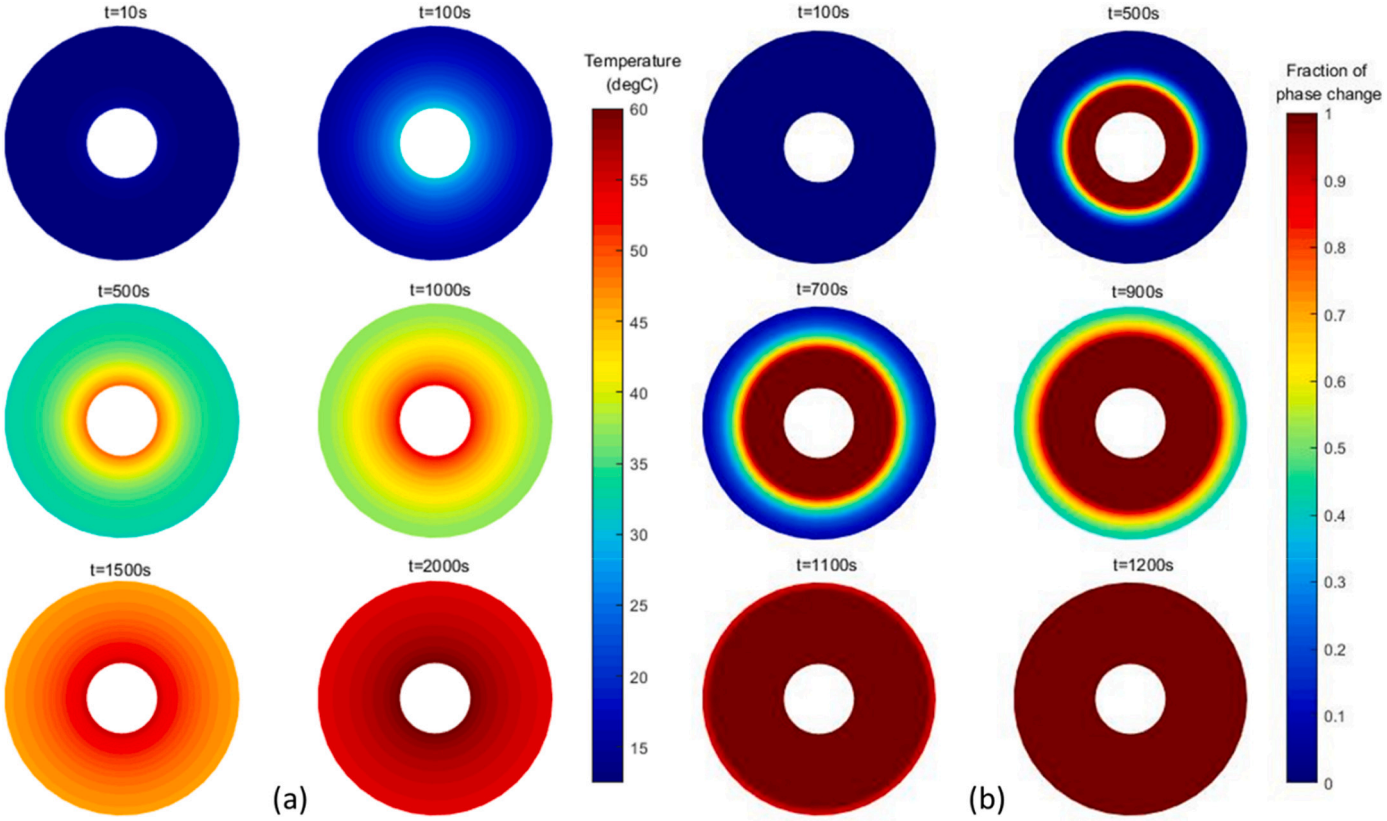

Fig. 10. Simulation results of phase change progress. (a)Temperature distribution of PCM section. (b) Fraction of phase change.

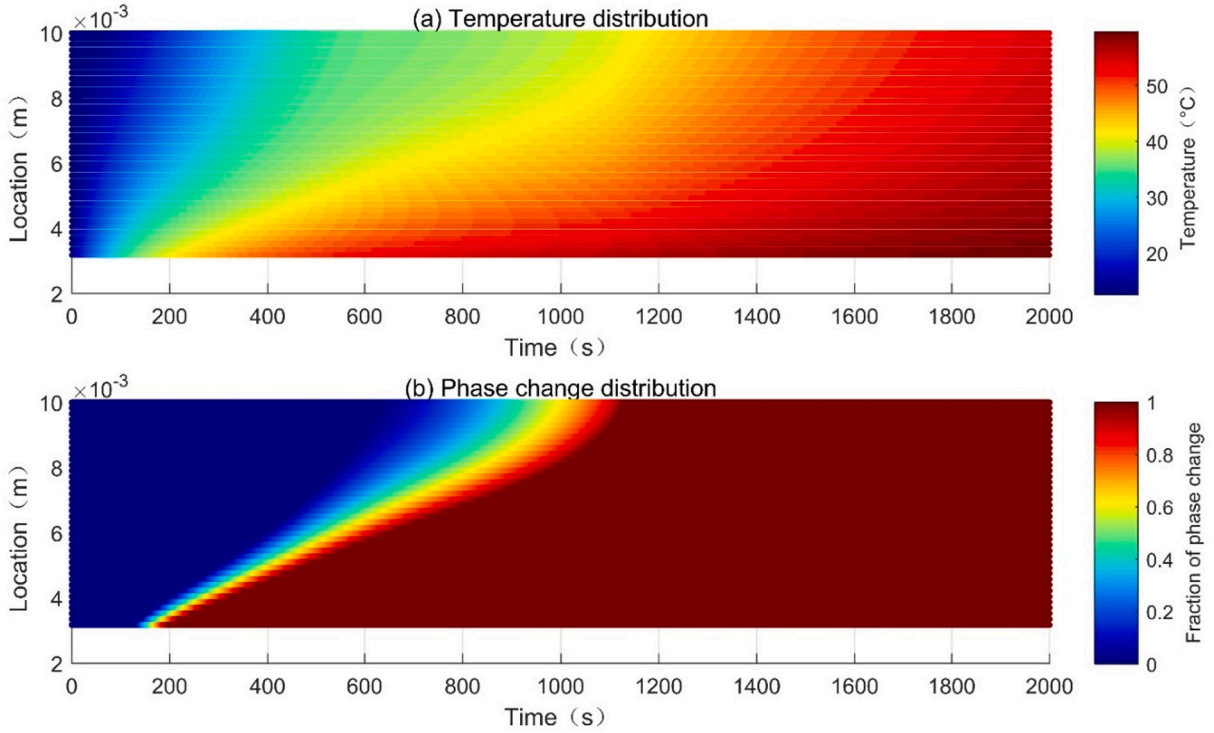

Fig. 11. Simulation results varied with time. (a) Temperature distribution of PCM section. (b) Fraction profile of phase change process.

(65 °C). As a result, the evaporator wall reached a near-constant temperature, while the condenser wall temperature (at r = 30 mm) was quickly increased from 12.5 °C to 36 °C in 150 s as the start-up process of TS. In stage 2, the phase change occurred; more heat was stored in the PCM in terms of latent heat, and the material achieved a jelly-like texture while still maintaining its form-stable ability from 150 to

1150 s. In this process, the condenser wall temperature increased from 36 °C to 60 °C in 80 s and then rose slowly. This might be because 1) the absorbed heat decreased as ΔT_{TS} reduced, or 2) there was an enhancement in the thermal resistance of the PCM near the condenser as the thermal conductivity became almost half of the original value after changing phase. The phase change first took place near the condenser wall and then spread along the radius direction of the FSPCM increasing the material's temperature. When the phase change process was completed, the FSPCM 'section's temperature exceeded 40 °C, and the fraction of phase change reached 1. In stage 3, the phase change process for the entirety of the PCM was completed after 1150 s. Moreover, the final temperature of the PCM remained uniform and reached a value as high as the condenser wall temperature as the heating time was sufficiently long. The sensible heat plays a vital role in this stage again.

Generally speaking, the temperature distribution had a similar trend to the phase change fraction profile during the whole heat transfer process, as shown in Fig. 11. This phenomenon is mainly due to the heat transfer mechanism of the FSPCM phase change process. The heat transfer process between each element is explicated in the previous section, and only conduction exists when the FSPCM absorbs heat. During this process, the specific heat capacity and latent heat of the material restrict the heat storage capacity of the device. At the same time, the thermal conductivity confines the heat transfer rate and the PCM temperature distribution associated with the thermosyphon's heat transfer ability.

4.4. Parameter analysis

Regarding the accuracy of the model, the effects of several factors, e.g., the evaporator length, the thermal conductivity, and latent heat of the PCM, were analyzed in order to investigate the heat transfer performance of the TS/FSPCM unit more comprehensively.

4.4.1. Effects of thermal conductivity of the PCM

As shown in Fig. 12, the effect of thermal conductivity was studied. The temperature distribution and phase change fraction were compared with different conditions as the thermal conductivity of the PCM increased from 0.38 to 1.5 W/(m•K). Noting that the thermal conductivities of the FSPCM varied with temperature, the values used in the simulation are listed in Table 5. For all cases, the temperature distribution had a similar profile for the phase change fractions of the PCM accordingly. The temperature gradient was smaller, with a larger heat transfer rate as higher thermal conductivity was achieved. The temperature profiles at the condenser wall (at $r = 30$ mm) for all cases are similar. This might be due to the heat transfer capacity of thermosyphon with constant temperature boundary conditions. Concretely speaking, the heat flux absorbed by the thermosyphon is determined by the temperature difference between the first element of PCM near the condenser and water bath, as explained in the numerical model of Section 2.2. Meanwhile, the profiles at $r = 100$ mm are quite different, because the heat is transferred along the radius direction, and the temperature rises faster with higher thermal conductivity.

As the thermal conductivity increases, the PCM will complete the phase change process faster (Fig. 13). In the figure above, when the average phase change fraction is equal to 0, the temperature of each point in the material is below the phase change temperature. In contrast, when the value equals one, it indicates that all the material has completed the phase change process. Although all the cases start to change phase at around 100 s due to the same heat capacity of PCM being applied, the duration of phase change decreases as the thermal conductivity increases. It takes around 1810 s, 1070 s, and 700 s for cases 1, 2, and 3 to change phases, respectively. This is due to the higher thermal conductivity, which causes a faster heat transfer rate when the latent heat is consistent.

4.4.2. Effects of latent heat of the PCM

The effect of the latent heat of the FSPCM on the heat transfer performance is demonstrated in Fig. 14. The thermophysical properties of the FSPCM were the same as those for the experimental samples, except

Table 5
Value of thermal conductivity of FSPCM used for simulation.

Conditions	Case 1	Case 2	Case 3
Thermal conductivity (at 30 °C)	0.38 W/(m•K)	0.75 W/(m•K)	1.50 W/(m•K)
Thermal conductivity (at 45 °C)	0.19 W/(m•K)	0.37 W/(m•K)	0.74 W/(m•K)

Note: Case 2 is the reference value measured in this paper, and case 1 halves this value while case 3 doubles this value in the scale.

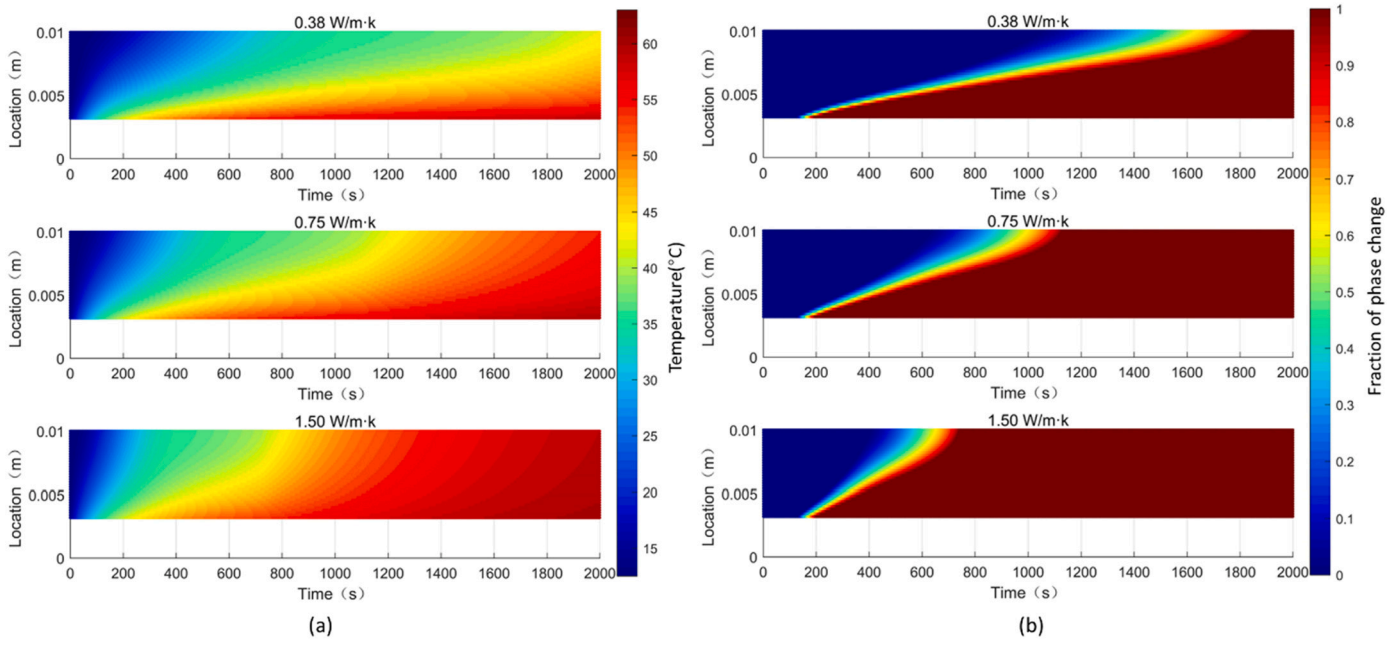

Fig. 12. Simulation results varied with the thermal conductivity of FSPCM. (a) Temperature distribution of PCM section. (b) Fraction profile of phase change process.

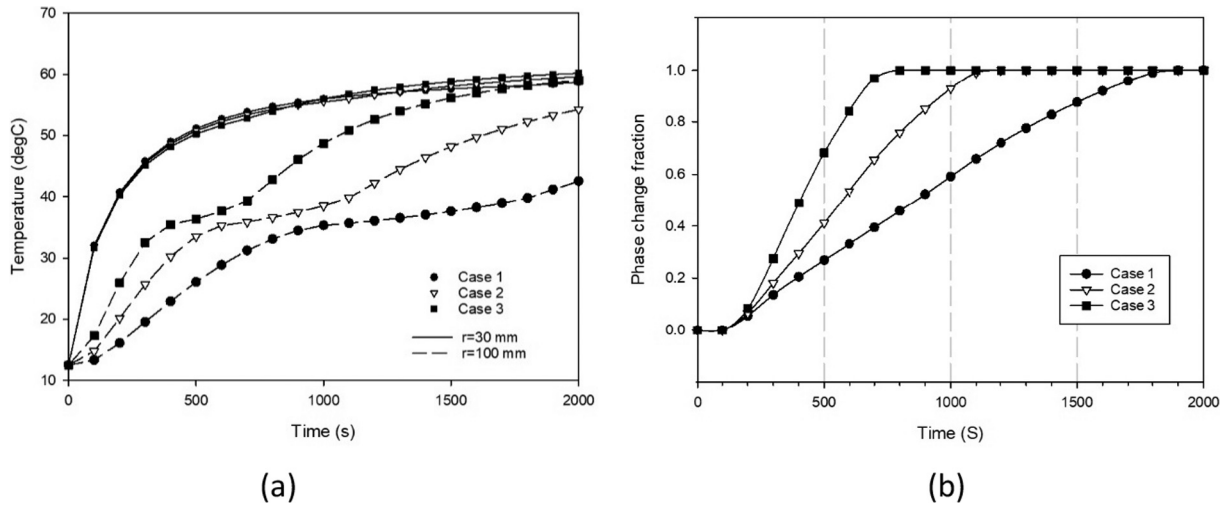

Fig. 13. (a) Temperature distribution in FSPCM. (b) The average phase change fraction of FSPCM.

that the latent heat was implemented as 136 kJ/kg, 160 kJ/kg, and 200 kJ/kg. As seen from the figure, the influence of latent heat on the heat transfer rate was insignificant. In other words, increasing latent heat has little impact on the temperature distribution of the PCM. Although it slightly delays the phase change end time, the trend and temperature gradient are almost consistent for all cases (shown in Fig. 15). The time for the average phase change fraction to reach 1 in 1170 s, 1230 s, and 1394 s, respectively. Moreover, the temperature profiles at the condenser wall are similar, and the temperatures at $r = 100$ mm are equvialent as the heating time is sufficient.

4.4.3. Effects of the length of the evaporator

To investigate the effect of the evaporator on the heat transfer performance of TS/FSPCM, additional experiments were conducted by placing the TS into the water bath with different values when the ambient temperature was 25 °C. The thermophysical properties of the FSPCM used for simulation were the same as in the PCM experimental samples. The experimental data were compared with simulation results shown in Fig. 16. Comparisons were performed altering the evaporator length,. As illuminated in Fig. 17, for which the initial temperature is set as 12.5 °C, the highest temperature with the 1-cm-long case is only around 38 °C, and it is 50 °C for the 2 cm case. The 1 cm case only negligibly starts to change phase from 1500 s. However, the FSPCM changes phase more quickly as the evaporator length increases. This is due to the total heat transfer area enhancement; thus, more heat can be transferred. However, the difference among the cases of a 5-cm-, 10-cm-, and 15-cm-long evaporator is minor. There might be two reasons for this. 1) Although the total heat transfer area increases, the heat transfer coefficiency of the evaporator section declines. Because the fill ratio decreases when the total mass of working fluid inside TS remains constant while increasing the evaporator length, this drives the coefficiency of the evaporator to fall based on reference [38]. 2) The boundary condition is a constant temperature for the evaporator side. Thus, the transferred heat flux mainly depends on the temperature difference between the evaporator and condenser sides. As the geometry of the condenser always remains constant, the heat transfer capacity of the PCM section 'won't change. The total heat transferred via TS is determined by the thermal resistance of the whole device. Therefore, there

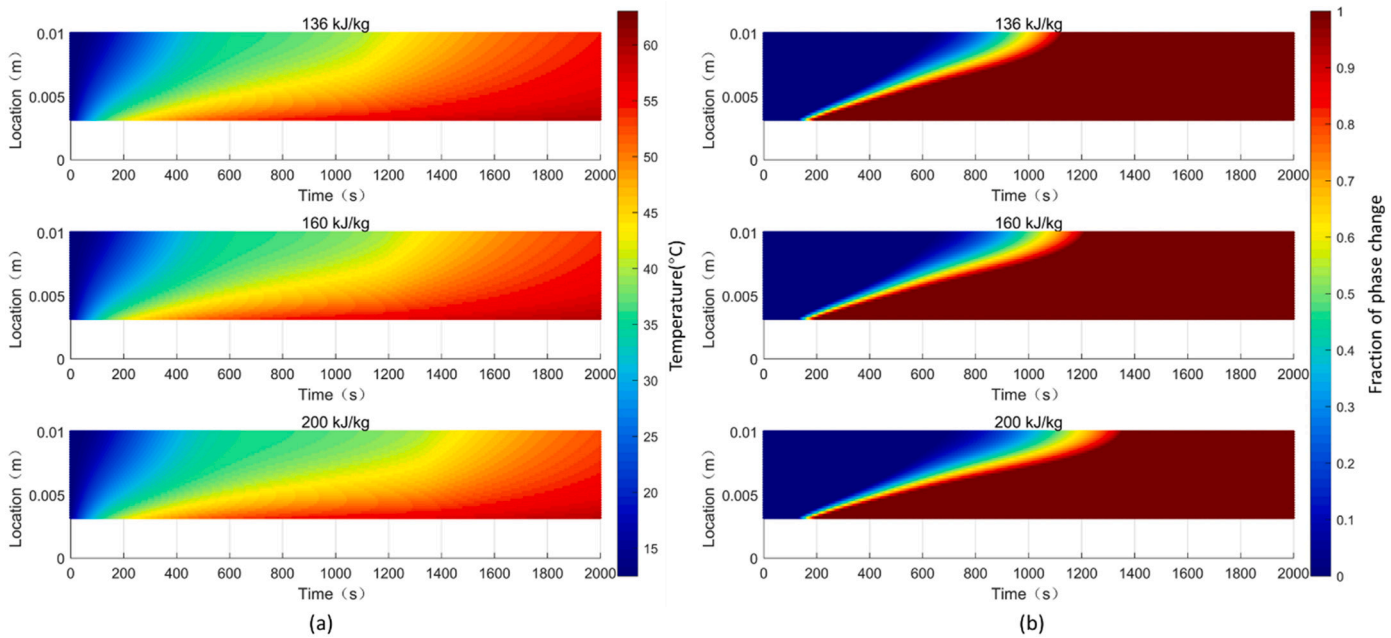

Fig. 14. Simulation results varied with the latent heat of fusion. (a) Temperature distribution of PCM section. (b) Fraction profile of phase change process.

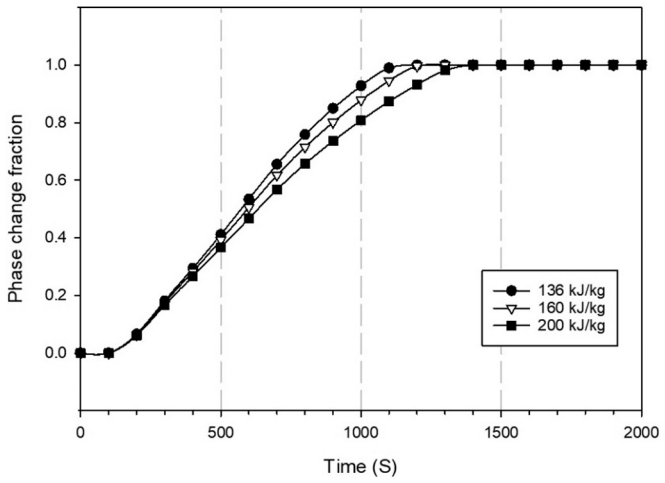

Fig. 15. The average phase change fraction of FSPCM varied with different latent heat values.

exists a heat flux limitation regardless of the length of the evaporator. Once it reaches the limit, the total heat absorbed achieves the maximum value. In other words, when the evaporator length is short, the major thermal resistance located in the evaporator section and the heat that can be stored are determined by the evaporator section. On the contrary, when the evaporator is long enough, the major thermal resistance goes to the condenser section, and the stored heat relies on the capacity of FSPCM.

5. Conclusions

This paper introduced and discussed the integration of FSPCM and TS acting as an innovative heat storage unit. Both numerical and experimental analyses were conducted to observe the heat transfer performance of the TS/FSPCM unit, including sensible and latent heat transfer. The average relative error between the experimental and model predictions was <3 %. The trends of the temperature distribution and phase change fraction of the FSPCM varying with time were also correctly captured. Meanwhile, the effects of the evaporator length, thermal conductivity, and latent heat of the FSPCM were analyzed using a numerical approach to investigate the unit's heat transfer performance more comprehensively. Regarding the research results, the following conclusions can be summarized:

(1) The thermal conductivity of the FSPCM plays a vital role in the TS/FSPCM unit. With more significant thermal conductivity, the overall phase change time becomes shorter, and the temperature gradient at each time step becomes smaller, while the condenser wall temperature increases more rapidly.
(2) Although the latent heat of the FSPCM affects the duration of the phase change process, the influence is minor. It takes 1170 s, 1230 s, and 1394 s to finish changing phase with 136 kJ/kg, 160

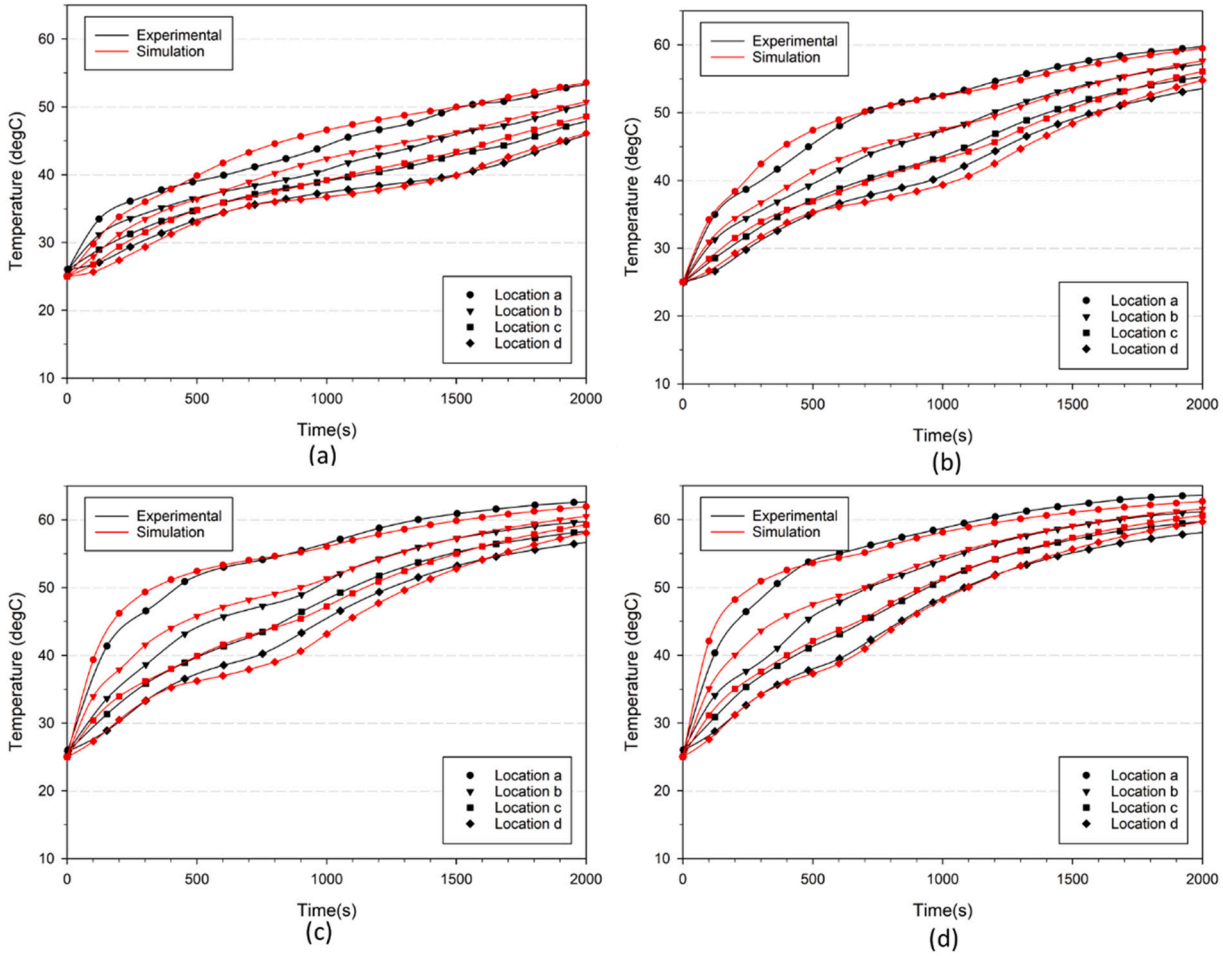

Fig. 16. Experiment and simulation results of different evaporator lengths.
(a) *Le* = 20 mm (b) *Le* = 50 mm (c) *Le* = 100 mm (d) *Le* = 150 mm.

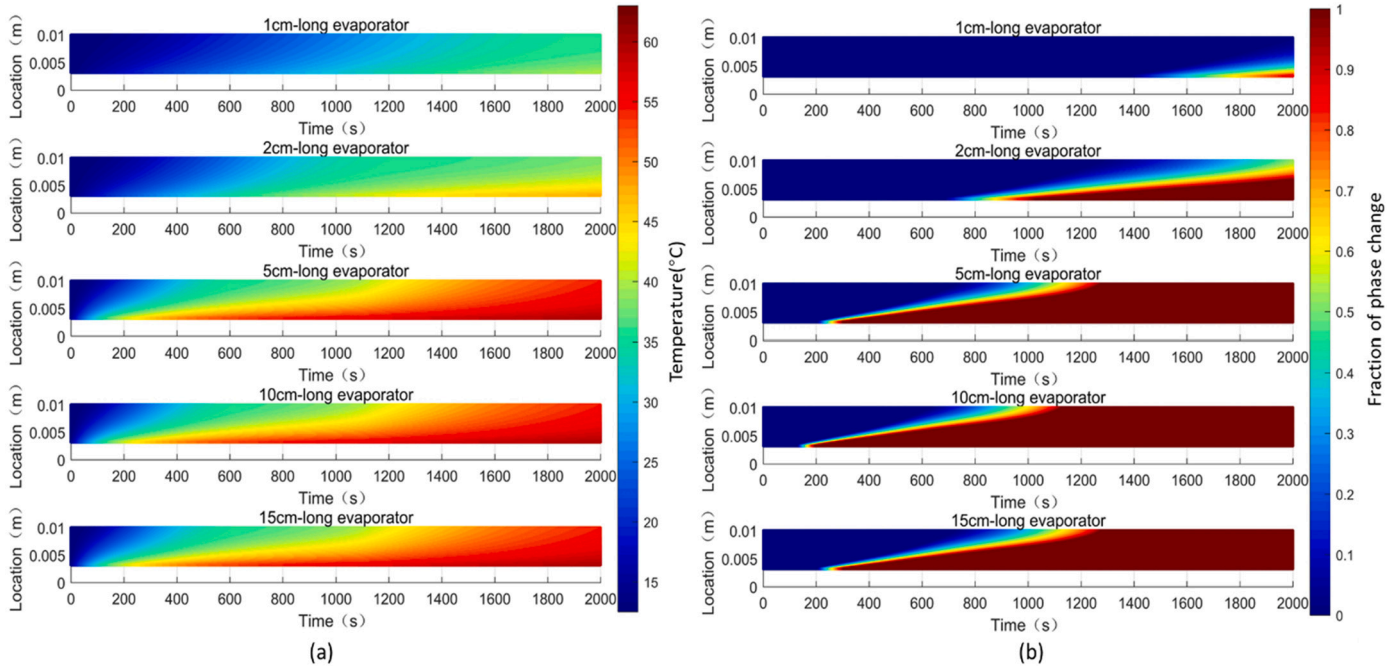

Fig. 17. Simulation results varied with evaporator length. (a) Temperature distribution of PCM section. (b) Fraction profile of phase change process.

kJ/kg, and 200 kJ/kg, respectively. The trend and temperature gradient are almost consistent for various latent heat values.

(3) There exists a critical value of the evaporator length that affects the thermal performance of the TS/FSPCM. When gradually increasing the evaporator length, the PCM changes phase faster. Once it exceeds the threshold, the effect decays.

CRediT authorship contribution statement

Wei Zhong: Conceptualization, Writing – original draft, Methodology. **Wandong Min:** Data curation, Validation, Investigation. **Xiaoling Cao:** Software. **Nan Zhang:** Resources. **Ziyu Leng:** Formal analysis. **Yanping Yuan:** Supervision. **Shady Attia:** Writing – review & editing.

Declaration of competing interest

The authors declare that they have no known competing financial interests or personal relationships that could have appeared to influence the work reported in this paper.

Data availability

Data will be made available on request.

Acknowledgments

The authors wish to thank the financial support of the National Natural Science Foundation of China (Grant No. 52106273) and Fundamental Research Funds for the Central Universities (Grant No. 2682021CX022).

References

[1] M.A. Habib, M. Hasanuzzaman, M. Hosenuzzaman, A. Salman, M.R. Mehadi, Energy consumption, energy saving and emission reduction of a garment industrial building in Bangladesh, Energy 112 (2016) 91–100.

[2] S. Rashidi, H. Shamsabadi, J.A. Esfahani, S. Harmand, A review on potentials of coupling PCM storage modules to heat pipes and heat pumps, J. Therm. Anal. Calorim. 140 (2020) 1655–1713.

[3] Y. Zhang, M. Umair, S. Zhang, B. Tang, Phase change materials for electron-triggered energy conversion and storage: a review, J. Mater. Chem. A 7 (2019) 22218–22228.

[4] K. Yu, Y. Liu, Y. Yang, Review on form-stable inorganic hydrated salt phase change materials: preparation, characterization and effect on the thermophysical properties, Appl. Energy 292 (2021), 116845.

[5] P. Lv, C. Liu, Z. Rao, Review on clay mineral-based form-stable phase change materials: preparation, characterization and applications, Renew. Sustain. Energy Rev. 68 (2017) 707–726.

[6] M.Q. Wu, S. Wu, Y.F. Cai, R.Z. Wang, T.X. Li, Form-stable phase change composites: preparation, performance, and applications for thermal energy conversion, storage and management, Energy Storage Mater. 42 (2021) 380–417.

[7] A. Papadimitratos, S. Sobhansarbandi, V. Pozdin, A. Zakhidov, F. Hassanipour, Evacuated tube solar collectors integrated with phase change materials, Sol. Energy 129 (2016) 10–19.

[8] R.J. Khan, M.Z.H. Bhuiyan, D.H. Ahmed, Investigation of heat transfer of a building wall in the presence of phase change material (PCM), Energy Built Environ. 1 (2020) 199–206.

[9] Y. Tomizawa, K. Sasaki, A. Kuroda, R. Takeda, Y. Kaito, Experimental and numerical study on phase change material (PCM) for thermal management of mobile devices, Appl. Therm. Eng. 98 (2016) 320–329.

[10] X. Guo, C. Liu, N. Li, S. Zhang, Z. Wang, Electro-thermal conversion phase change composites: the case of polyethylene glycol infiltrated graphene Oxide/Carbon nanotube networks, Ind. Eng. Chem. Res. 57 (2018) 15697–15702.

[11] W. Aftab, A. Mahmood, W. Guo, M. Yousaf, H. Tabassum, X. Huang, Z. Liang, A. Cao, R. Zou, Polyurethane-based flexible and conductive phase change composites for energy conversion and storage, Energy Storage Mater. 20 (2019) 401–409.

[12] Y. Lin, Y. Jia, G. Alva, G. Fang, Review on thermal conductivity enhancement, thermal properties and applications of phase change materials in thermal energy storage, Renew. Sustain. Energy Rev. 82 (2018) 2730–2742.

[13] I. Jmal, M. Baccar, Numerical study of PCM solidification in a finned tube thermal storage including natural convection, Appl. Therm. Eng. 84 (2015) 320–330.

[14] J. Zhao, Z. Rao, C. Liu, Y. Li, Experimental investigation on thermal performance of phase change material coupled with closed-loop oscillating heat pipe (PCM/CLOHP) used in thermal management, Appl. Therm. Eng. 93 (2016) 90–100.

[15] W. Li, H. Wan, T. Jing, Y. Li, P. Liu, G. He, F. Qin, Microencapsulated phase change material (MEPCM) saturated in metal foam as an efficient hybrid PCM for passive thermal management: a numerical and experimental study, Appl. Therm. Eng. 146 (2019) 413–421.

[16] S.L. Tariq, H.M. Ali, M.A. Akram, M.M. Janjua, M. Ahmadlouydarab, Nanoparticles enhanced phase change materials (NePCMs)-a recent review, Appl. Therm. Eng. 176 (2020), 115305.

[17] H.M. Ali, Applications of combined/hybrid use of heat pipe and phase change materials in energy storage and cooling systems: a recent review, J. Energy Storage 26 (2019), 100986.

[18] M.S. Naghavi, K.S. Ong, M. Mehrali, I.A. Badruddin, H.S.C. Metselaar, A state-of-the-art review on hybrid heat pipe latent heat storage systems, Energy Convers. Manag. 105 (2015) 1178–1204.

[19] D. Etheridge, K. Murphy, D. Reay, A PCM/heat pipe cooling system for reducing air conditioning in buildings: review of options and report on field tests, Build. Serv. Eng. Res. Technol. 27 (2006) 27–39.
[20] R. Dhumane, A. Mallow, Y. Qiao, K.R. Gluesenkamp, S. Graham, J. Ling, R. Radermacher, Enhancing the thermosiphon-driven discharge of a latent heat thermal storage system used in a personal cooling device, Int. J. Refrig. 88 (2018) 599–613.
[21] G. Murali, K. Mayilsamy, T. Arjunan, An experimental study of PCM-incorporated thermosyphon solar water heating system, Int. J. Green Energy 12 (2015) 978–986.
[22] W. Wu, X. Yang, G. Zhang, K. Chen, S. Wang, Experimental investigation on the thermal performance of heat pipe-assisted phase change material based battery thermal management system, Energy Convers. Manag. 138 (2017) 486–492.
[23] W. Zhong, W. Ji, Applications of coupling thermosyphons with phase change materials: a review, Energy Build. 233 (2020), 110690.
[24] S. Filippeschi, Comparison between miniature periodic two-phase thermosyphons and miniature LHP applied to electronic cooling equipment, Appl. Therm. Eng. 31 (2011) 795–802.
[25] M.S. El-Genk, H.H. Saber, Determination of operation envelopes for closed, two-phase thermosyphons, Int. J. Heat Mass Transf. 42 (1999) 889–903.
[26] A. Faghri, M.M. Chen, M. Morgan, Heat transfer characteristics in two-phase closed conventional and concentric annular thermosyphons, J. Heat Transf. 111 (1989) 611–618.
[27] T. Fujita, T. Ueda, Heat-transfer to falling liquid-films and film breakdown-I: subcooled liquid-films, Int. J. Heat Mass Transf. 21 (1978) 97–108.
[28] T. Fujita, T. Ueda, Heat-transfer to falling liquid-films and film breakdown -II: saturated liquid-films with nucleate boiling, Int. J. Heat Mass Transf. 21 (1978) 109–118.
[29] M.S. ElGenk, H.H. Saber, Heat transfer correlations for small, uniformly heated liquid pools, Int. J. Heat Mass Transf. 41 (1998) 261–274.
[30] A. Faghri, Heat Pipe Science and Technology, Second ed., Global Digital Press, 2016.
[31] H. Nguyen-Chi, M. Groll, Entrainment or flooding limit in a closed two-phase thermosyphon, J. Heat Recov. Syst. 1 (1981) 275–286.
[32] S. Noie, M. Sarmasti Emami, M. Khoshnoodi, Effect of inclination angle and filling ratio on thermal performance of a two-phase closed thermosyphon under normal operating conditions, Heat Transfer Eng. 28 (2007) 365–371.
[33] W. Zhong, T. He, T. Butcher, R. Trojanowski, S. Mamalis, T. Wagner, Y. Chudnovsky, W. Worek, Y. Wang, J.P. Longtin, Falling-film thermosyphons: application to water harvesting from humid gas streams, Int. J. Heat Mass Transf. 164 (2021), 120486.
[34] T.L. Bergman, F.P. Incropera, D.P. DeWitt, A.S. Lavine, Fundamentals of Heat and Mass Transfer, John Wiley & Sons, 2017.
[35] H. Imura, H. Kusuda, J. Ogata, T. Miyazaki, N. Sakamoto, Heat transfer in two-phase closed-type thermosyphons, JSME Trans. 45 (1979) 712–722.
[36] Y. Jin, Preparation and Temperature Control Properties of Thermochromic Flexible Form-stable Phase Change Materials, Southwest Jiaotong University, 2018.
[37] ASHRAE Guideline 14-2002 , Measurement of Energy and Demand Savings, n.d.
[38] B. Jiao, L.M. Qiu, X.B. Zhang, Y. Zhang, Investigation on the effect of filling ratio on the steady-state heat transfer performance of a vertical two-phase closed thermosyphon, Appl. Therm. Eng. 28 (2008) 1417–1426.